ASCE Journal of Geotechnical & Geoenvironmental Engineering, Vol. 143, No. 9,
published online Dec. 16, 2017, https://doi.org/10.1061/(ASCE)GT.1943-5606.0001841

Influence of Particle Morphology on the Friction and Dilatancy of Sand

Khalid A. Alshibli[1] and Mehmet B. Cil[2]

ABSTRACT: The shear strength of granular materials is influenced by many factors that include particle morphology, gradation, mineralogy, fabric, material density, applied stresses, boundary conditions and loading path. In recent years, 3D imaging techniques such as computed tomography enabled researchers to quantify sand particle morphology based on 3D images of particles. This paper presents an experimental investigation of the influence of particle morphology (i.e., surface texture, roundness, form, and sphericity), specimen density, and initial mean stress on the shear strength properties of dry specimens of silica sands and glass beads. Spherical glass beads as well as three other sands (with different morphologies) with grain sizes between US sieve #40 (0.42 mm) and sieve #50 (0.297) where tested at 15, 50, 100, and 400 kPa confining pressures under axisymmetric triaxial compression. The influence of particle morphology on stress-strain response, volume change behavior as well as peak state and critical state (CS) friction, and dilatancy angles was examined. The triaxial test results of Toyoura and Hostun RF sands collected from the literature was included in the analyses. Simple statistical models capable of predicting the peak and CS friction angles as well as dilatancy angle by providing particle surface texture, roundness, sphericity, relative density and initial mean stress as input parameters were developed. The results show that morphology parameters highly influence dilatancy angle, CS and peak state friction angles.

Key Words: shear strength, shape, roundness, dilatancy, granular materials, triaxial experiments

[1] Professor, Dept. of Civil & Env. Engineering, 325 John Tickle Building, University of Tennessee, Knoxville, TN 37996, USA, Tel. 011-865-974-7728, Email: Alshibli@utk.edu
[2] Postdoctoral Research Fellow, Dept. of Civil & Env. Engineering, Technological Institute, 2145 Sheridan Road, Tech A236, Northwestern University, Evanston, IL 60208, USA, Email: mehmet.cil@northwestern.edu

INTRODUCTION

The shear strength of uncemented granular materials is attributed to the true friction, particle rearrangement/interlocking (dilatancy effects), and crushing if the material is tested under very high compressive mean stresses. During shearing, particles may interlock, translate, and/or rotate as they interact with each other. Granular materials consist of discrete particles with fabric (microstructure) that changes during loading. All particle-scale interactions are strongly influenced by the morphology of particles (i.e., size, shape and surface characteristics) which therefore plays a critical role on the constitutive behavior and deformation characteristics of uncemented granular materials. The quantitative description of morphology, fabric, and particle interactions in the context of granular materials is well understood in 2D, and has been studied extensively since the early 1970s (e.g., Oda 1972; Powers 1982; Kanatani 1984; Frost & Kuo 1996); however, similar 3D measurements are still very limited. Cho *et al.* (2006) investigated the influence of particle morphology on stiffness and strength of a large database of sand. Sphericity and roundness were visually characterized using 2D microscopic images of the sands. They concluded that increasing particle irregularity results in an increase in the CS friction angle. Cho *et al.* (2006) further stated, "Particle shape emerges as a significant soil index property that needs to be properly characterized and documented, particularly in clean sands and gravel. The systematic assessment of particle shape will lead to a better understanding of sand behavior."

Morphology (shape, form, sphericity, and surface roughness) and gradation of particles significantly influence the strength and deformation properties of granular materials. Sands with a predominance of angular particles possess greater friction than those consisting mainly of rounded particles. Koerner (1968) investigated the effects of angularity, gradation and mineralogy on shear strength of cohesionless soils and found that the angle of internal friction increases with

increasing angularity of particles, and decreases with increasing effective size. Most current experimental studies rely on 2D characterization of particle shape and sphericity in assessing their influence on the shear strength of granular materials (e.g., Sukumaran and Ashmawy 2001, Alshibli and Alsaleh 2004; Cho *et al.* 2006; Guo and Su 2007). Based on limited experimental measurements, Alshibli and Alsaleh (2004) found that the peak friction and dilatancy angle increase as particle surface roughness and angularity increase. However, the results were inconclusive because particle shape and sphericity were not quantified from 3D images. More sand with wide range of morphology classes and densities need to be tested under different confining pressures while imaged in 3D and analyzed to identify the contribution of these factors to the friction and dilatancy of granular materials. In summary, the literature lacks a systematic 3D study that experimentally investigates the effects of particle morphology on the friction and dilatancy of sheared sand.

The objective of this paper is to quantify the influence of particle surface texture, roundness, and form on the peak and CS friction angles, and dilatancy of uniform silica sands. Roundness, form and sphericity of sand particles and glass beads were quantified from high-resolution 3D images. The objective here is to develop simple and practical statistical models that incorporate the influence of particle morphology, initial mean stress and specimen density to predict the peak friction angle, CS friction angle and dilatancy angle.

SAND MORPHOLOGY AND PHYSICAL PROPERTIES

Three types of silica sand known as F-35 Ottawa sand, #1 Dry Glass sand, and GS#40 Columbia grout sands were acquired and only grain size between US sieves #40 (0.429 mm) and #50 (0.297 mm) were used in this study (Table 1). They represent uniform silica sands with

different morphologies ranging from rounded to angular particle classes. Glass beads with similar grain size as these sands are also included in the investigation to provide baseline measurements for surface texture, roundness and form (Figure 1).

A definition of particle shape in terms of sphericity and roundness is widely accepted. However, methods have not been standardized because of the tedious task of taking numerous readings. Wadell (1932) was the first to point out that the terms *shape* and *roundness* were not synonymous, but rather include two geometrically distinct concepts. Zavala (2012) presented a review of particle shape indices reported in the literature. Also, Alshibli et al. (2014) presented a literature review of particle morphology and proposed sphericity (I_{sph}) and roundness (I_R) indices of sand particles based on 3D synchrotron micro computed tomography (SMT) images of particles. They are defined as:

$$I_{sph} = \frac{V_p}{V_s} \tag{1}$$

$$I_R = \frac{A_p}{4\pi(\frac{d_L+d_I+d_S}{6})^2} \tag{2}$$

$$\text{Form, } F = d_S / d_L \tag{3}$$

Denominator in Eq. (2) represents the surface area of a sphere that has a diameter equals to the average of the shortest (d_S), intermediate (d_I), and longest (d_L) lengths of the particle that pass through the center of mass of the particle. V_p and V_s are the actual volume of the particle and the volume of sphere with a diameter equals to d_S, respectively. I_{sph} equals to unity for spherical particle. A_p is the actual 3D surface area of the particle. I_R equals to unity for a particle that has no corners on its surface and has the shape of a sphere. F is a measure of elongation of a particle and can range from a very small value for platy particles to 1 for a sphere. Hundreds of particles (see

Table 2 were used to in the analysis to calculate I_{sph}, I_R, $a$and F. A minimum of 400 particles need to be analyzed to produce statistically representative morphology parameters. Also, Alshibli et al. (2014) measured surface texture of sand particles using optical interferometry technique and calculated the root mean square texture (R_q) as follows:

$$R_q = \sqrt{\frac{1}{MN}\sum_{i=1}^{M}\sum_{j=1}^{N} Z_{ij}^2} \quad (4)$$

Where M and N are the number of pixels in X and Y direction, Z_{ij} is the surface height at a specific pixel relative to the reference mean plane. R_q represents the standard deviation of the surface heights. Table 2 lists the morphology indices of the sands. In addition, samples of Toyoura and Hostun RF sands were analyzed in the study along with other sands (Figure 2). Toyoura sand is a poorly graded silica sand with a mean particle size (d_{50}) of 0.22 mm and has been extensively tested by Japanese geotechnical researchers under many loading and state conditions. Hostun RF sand is also a poorly graded sand with d_{50} = 0.34 mm and has been widely tested by many geotechnical researchers in France under various loading paths.

SPECIMEN PREPARATION AND TEST PROCEDURE

Air pluviation, vibration and tamping are common techniques used in sand specimen preparation. Air pluviation (raining) is perhaps the best method for preparing homogeneous laboratory specimens with the desired density to simulate the natural soil fabric occurring due to sedimentation. A specified target density or void ratio for the specimen can be obtained by varying the intensity of raining and the drop height. Detailed description of this technique has been presented by Miura and Toki (1982), Rad and Tumay (1987) and Al-Shibli et al. (1996). The air pluviation apparatus of Al-Shibli et al. (1996) was used to prepare the medium dense and very

dense specimens for the experiments reported in this paper (Figure 3). Dry sand flows out of a funnel with an opening diameter (d) and get diffused through four US No. 4 sieves with openings staggered at 45°. By changing the height of drop (H) between the bottom of the sieves and the top of the specimen mold, and d, a wide range of densities may be obtained repeatedly with minimum variation. Loose specimens were prepared using a procedure like ASTM-D4254 where a funnel with 13 mm spout was held in hand and sand was deposited from a drop height of 25 mm.

The maximum and minimum index densities of tested sands were measured according to ASTM-D4253 and ASTM-D4254 standard procedures, respectively. It is interesting to report that air pluviation technique employed in this study can produce specimens with densities higher than the maximum index density (or minimum void ratio, e_{min}) of ASTM-D4253 procedure. Table 1 lists the values of e_{max} and e_{min} based on ASTM standard procedures along with the minimum void ratio according to Al-Shibli et al. (1996) (e_{min}_A). Lo Presti et al. (1992) reported that ASTM-D4253 may not produce the densest case for some sands and it is possible to prepare specimens with relative density, $D_r > 100\%$.

Cylindrical specimens measure 71.1 mm in diameter and 142.2 mm in height were prepared by dry air pluviation (raining) of the sand into a mold. End platens with a diameter of 100 mm and tungsten carbide facing were used in the experiments. Using end platens larger than the initial specimen diameter allows lateral expansion of specimen with minimal friction between a highly-polished tungsten carbide facing and the sand particles. The triaxial test cell was assembled around the specimen, filled with water, and pressurized to apply the desired confining pressure (σ_3). Quasi-static triaxial compression experiments were conducted on dry specimens using a conventional triaxial system with very precise measurements and controls for the axial load, axial displacement, confining pressure, and bulk volumetric changes. The deviator stress was applied at

a constant displacement rate of 0.5 mm/minute. The volume change of the specimen was measured by tracking the changes in the volume of water pumped in/purged out of cell water while maintaining a constant σ_3 during the experiments. Table 3 list a summary of the experiments. Using e_{min} of ASTM-D4253 to calculate D_r resulted in values in the range of 120% - 165% for the very dense specimens; therefore, D_r was calculated using e_{max} and e_{min}_A.

STRESS-STRAIN AND VOLUMETRIC STRAIN BEHAVIOR

The principal stress ratio (PSR = σ_1 / σ_3) versus axial strain, and volumetric strain versus axial strain relationships for the glass beads and the sands are depicted in Figures 4 through 7. Volume expansion is taken negative in this paper. The PSR of loose specimens of glass beads (Figure 4a) gradually increased until reaching a CS value where there is no increase in PSR with further shearing. The volumetric strain exhibited a dilative behavior from the beginning for the specimen tested at σ_3 = 15 kPa and a small contraction followed by dilation for specimens tested at σ_3 = 50, 100, and 400 kPa, with negligible difference in volumetric strains between these experiments. As the specimen density increases, the PSR increases and a peak state emerges (Figure 4b&c) followed by a drop in PSR and eventually reaching a CS. A higher density and a low confining pressure cause a higher peak PSR followed by more pronounced softening. Figure 4b&c also shows that the specimens exhibit a dilative behavior after a very small initial contraction for all confining pressures with the volume expansion being higher for the very dense cases and the amount of volume increase decreases as the confining pressure increases. The PSR of glass beads exhibited an oscillatory behavior during the post-peak regime (if a specimen exhibits a peak state) or when the PSR reaches a CS. This behavior is attributed to the slip-stick behavior between the particles as they shear against each other. Glass beads have relatively uniform

roundness/sphericity and smoother surface which causes the slip-stick that caused an oscillation in PSR. Alshibli and Roussel (2006) presented a detailed experimental study of slip-stick behavior of glass beads.

The specimens exhibit a volume increase after an initial contraction for loose specimens (Figures 5a, 6a, & 7a) or dilation from the beginning of the experiment for medium dense and very dense sand specimens. For the medium dense and very dense cases, the rate of dilation began high and decreased at high strains to approach a CS. On the other hand, loose specimens exhibited an initial contractive behavior followed by a small rate of dilation until the end of the experiment. Using sand with a narrow grain size gradation caused the specimen to stay active as shearing continued which explains a small volume increase as shearing continued. Batiste et. al (2004) and Alshibli et al. (2016) reported a detailed investigation of failure mode of triaxial specimens that were monitored using computed tomography imaging technique, that revealed specimens continued to shear along secondary active shear bands as shearing continued.

Sieve analysis was conducted on the specimens tested at σ_3 = 400 kPa after the tests to determine the percentage of sand fractured during the test and the results are listed in Table 3. #1 Dry glass sand has the highest percentage of fractured sand at about 11.4% to 12.3%. Such analyses revealed that specimen density (i.e., loose, medium dense, or very dense) has no influence on the percentage of fractured sand. In all cases, fresh batches of sand were used for each experiment to eliminate the possibility of using sand with sheared asperities of fractured particles.

The uniqueness of the CS line for the same type of sand is still a controversial topic (Wood 1990; Konrad 1990; Riemer and Seed 1997; Shipton and Coop 2014). The CS line for sand is curved in the $e = \log(p')$ plane and a few researchers proposed a linear representation of a

modified CS line. For example, Li and Wang (1998) proposed a linear representation of the CS line for Toyoura sand by plotting e versus log $(\frac{p'}{p_{atm}})^{0.7}$ where p_{atm} is atmospheric pressure. It is clear from Figures 4 through 7, that the sands and glass beads did not reach a unique CS. To illustrate the non-uniqueness of CS for sand, Figure 8 displays the relationship between mean effective stress at the CS (p'_{cs}) versus deviator stress at the CS (q_{cs}) along with the variation of void ratio versus nominal axial strain for F-35 sand. It is obvious that specimen density and stress state affect CS of sand and once should include the influence of p' and specimen density in predicting the CS friction angle.

INFLUENCE OF PARTICLE MORPHOLOGY ON VOID RATIO

Particle morphology affects the packing density of granular materials. The relationship between (e_{max} - e_{min_A}) and R_q, I_{sph}, I_R, and F were investigated and we found no clear trend between (e_{max} - e_{min_A}) and R_q, I_{sph}, or I_R. On the other hand, (e_{max} - e_{min_A}) has a clear trend with F as depicted in Figure 9 where e_{max} - e_{min_A} exhibit a steep almost linear decrease with the increase of F for the sands and a much smaller rate of decrease as F approaches 1 for glass beads. Abbireddy and Clayton (2010) used PFC2D discrete element code to generate cylindrical, triangular, diamond, and platy particles using overlapping discs with a constant diameter. Clump logic of PFC2D was used to generate the particles. Abbireddy and Clayton (2010) defined form as the ratio of the largest inscribing circle to that of the smallest circumscribing circle; a similar definition to Eq. 3 recognizing that Eq. 3 uses 3D images of particles. The results of Abbireddy and Clayton (2010) for double-layered platy particles are also included in Figure 9. The trend of calculated e_{max} - e_{min_A} values of Abbireddy and Clayton (2010) is similar to the experimental measurements for sands and glass beads with a shift. Such difference is attributed to the shape of 2D platy particles

that were used in Abbireddy and Clayton (2010) calculations versus 3D measurements of natural granular materials.

FRICTION AND DILATANCY ANGLES

In 1776, Coulomb suggested that soil resistance to shearing is dependent on the applied normal stress and can be modeled using a simple sliding block model (Coulomb 1776). It is a purely static relationship that totally ignores the kinematic or dilatancy contribution to the strength of granular materials. Reynolds (1885, 1886) is credited as the first researcher to introduce the concept of dilatancy property of granular materials. Then, Hansen (1958) defined dilatancy angle as the ratio of plastic volume change divided by the plastic shear strain. This concept opened the door for more research that emphasized the importance of dilatancy effects in understanding the constitutive behavior and describing the failure of granular materials (e.g., Rowe 1962; Roscoe 1970; Vermeer 1978; Vardoulakis & Graf 1985; Manzari & Dafalias 1997; Alsaleh *et al.* 2006). Rowe (1962) advocated the importance of dilatancy in describing the peak stress state in granular materials. Rowe's theory assumes ideal spherical particles with only inter-particles sliding in 2D and ignores particle rotation.

The peak state friction angle (φ_p) and CS friction angle (φ_{cs}) were calculated from the peak and CS PSR, respectively as:

$$sin\varphi = \frac{PSR-1}{PSR+1} \tag{5}$$

The dilatancy angle (ψ) was calculated using the following relationship (Vermeer and de Borst, 1984):

$$sin\psi = \frac{(d\varepsilon_v/d\varepsilon_1)}{2+(d\varepsilon_v/d\varepsilon_1)} \tag{6}$$

Where $d\varepsilon_v/d\varepsilon_1$ is the slope of volumetric strain (ε_v) versus axial strain (ε_1) at the highest rate of dilation from the nominal axial strain versus volumetric strain relationship, taken as positive slope for dilation to yield a positive dilatancy angle. Bolton (1986) defined the difference between φ_p and φ_{cs} as a function of ψ of the material. He proposed an empirical statistical model that relates φ_p and $\varphi_{cs}$to ψ for sands based on experimental data as:

$$\varphi_p - \varphi_{cs} = 0.5\,\psi = 3I_{RB} \qquad \text{for triaxial experiments} \tag{7a}$$

$$I_{RB} = D_r\,(10 - lnp') - 1 \tag{7b}$$

where I_{RB} is an empirical relative dilatancy index, and $p' = (\sigma_1' + 2\sigma_3')/3$ is the mean effective stress at CS in kPa. Tatsuoka (1987) criticized Bolton's (1986) model for ignoring the anisotropic behavior of sand caused by a preferred deposition direction (fabric effect) during specimen preparation. In other words, Tatsuoka (1987) emphasized the importance of incorporating the influence of fabric in any model to describe friction and dilatancy properties of granular materials. Furthermore, Chakraborty and Salgado (2010) stated that the Bolton (1986) model does not capture the behavior of sand well for low confining pressure and proposed a modified version of Bolton (1986) models. Hasan and Alshibli (2010) found that Eq. 7 fails to capture the behavior of very angular granular materials tested under very low confining pressure and proposed a new statistical model. Figure 10 displays Bolton (1986) prediction (Eq. 7) versus experimental measurements of $\varphi_p - \varphi_{cs}$ of the results reported in this paper, which clearly show that there is a wide scatter of values and Bolton model over-predicted $\varphi_p - \varphi_{cs}$. Bolton (1986) model gave better prediction for experiments that were conducted at high confining pressure (σ_3 = 400 kPa) which are shown using filled triangles in Figure 10.

The loading condition (i.e, plane strain, axisymmetric triaxial, true triaxial, etc.), direction of principal stress with respect to specimen axis, and the ratio of applied principal stresses affect shear strength of soils (Kandasami and Murthy 2015, 2017). Axisymmetric triaxial compression procedure was selected in this paper to perform the experiments since it is the most common procedure and has been widely used to characterize shear strength of soils. Axisymmetric triaxial compression does not allow a variation of the intermediate principal stress ratio known as b-value and represents the lower limit of b-value (b = 0). One needs a true triaxial or a hollow cylinder torsion testing system to investigate the influence of b-value on friction and dilatancy angles. Also, particle morphology affects soil fabric which defines the arrangement of particles, particle groups and associated pore space. One can incorporate the influence of fabric by defining a fabric tensor that can be incorporated in a constitutive model that accounts for fabric. However, the objective of this paper is to develop simple statistical models to quantify the influence of particle morphology on friction and dilatancy angles. The authors performed individual assessment of the influence of quantitative parameters such as I_R, I_{sph}, F, R_q, D_r and normalized mean effective stress (p'_o/p_{atm}) on φ_p, φ_{cs} and ψ. F gave better correlation than I_{sph}; therefore, F will be used an index to represent particle sphericity. The results of the analysis are shown in Figure 11 where predictor D_r shows a positive trend with φ_{cs} whereas F, I_R, and p'_o/p_{atm} show a negative trend. R_q shows a positive trend if all measurements are considered and a negative trend if only sand data are used.

It appears that I_R , F, R_q, p'_o/p_{atm} D_r affect φ_p, φ_{cs} and ψ. Therefore, linear multiple regressions were conducted where function for each of the multiple regressions took the form of:

$$f\left(x_j^i, \beta_j\right) = \beta_1 x_1^i + \beta_2 x_2^i \cdots \beta_K x_k^i \text{ where } i = \{1,2,\dots,N\} \text{ and } j = \{1,2,\dots,K\} \quad (8)$$

Where β_j is an estimate for each of the $N = 5$ coefficients for each predictor value x. Statistical estimation and inference in multivariable regressions focuses on regression coefficients β_j, which were evaluated using Levenberg-Marquardt least squares algorithm, a commonly used algorithm in least square curve fitting problems. It optimizes regression coefficients β_j of the model curve $f(x_j^i, \beta_j)$ such that the sum of squares of the deviations, $S(\beta_j)$ is minimized

$$minimize \left\{ S(\beta) = \sum_{i=1}^{N} [y^i - f(x_j^i, \beta_j)]^2 \right\} \tag{9}$$

Where y is the dependent variable (φ_{cs}, φ_p, or ψ). Standard error of estimate (SE) is a measurement of error in the estimated regression coefficient. Therefore, a smaller SE value indicates less deviation in the predicted value. SE is an extension of the definition of simple linear regression which is defined as:

$$SE(\beta_j) = \sqrt{C_{jj}} \tag{10}$$

Where C is the variance-covariance matrix of the estimated regression coefficients, which is defined as:

$$C = \sigma^2 (X^T X)^{-1} \tag{11}$$

Where X is the matrix of independent variables (x_j^i), σ is the standard deviation of the entire predicted data, which can be expressed as:

$$\sigma^2 = \sum_{i=1}^{N} (y_i - y_i')^2 \Big/ (N - K) \tag{12}$$

Where Y' is the vector of predicted dependent variables. $N - K$ is the degrees of freedom of the regression model. *P*-value is used to evaluate the significance of an individual regression

coefficient in term of the contribution of a variable while other variables are included in the model. For example, a *P*-value of 5% means there is only 5% probability that the model results are random or there is a 95% probability that the model results are being correct that the independent variable has a significant effect on the regression model.

Predictors were individually analyzed in conjunction with φ_{cs}, φ_p, and ψ that gave the following models:

$$\varphi_{cs} = 23 - 134.06\,F + 142.04\,I_R - 21.02\,R_q - 0.861\left(\frac{p'_o}{p_{atm}}\right) + 0.043\,D_r \quad (13)$$

$$\varphi_p = 23 + -62.90\,F + 67.00\,I_R - 9.02\,R_q - 0.932\left(\frac{p'_o}{p_{atm}}\right) + 0.160\,D_r \quad (14)$$

$$\psi = 77.72\,F - 76.35\,I_R + 12.77\,R_q - 0.486\left(\frac{p'_o}{p_{atm}}\right) + 0.196\,D_r \quad (15)$$

The true angle of friction (φ_μ) defines the friction between mineral surfaces of the materials and has a value of 23° for silica (Rowe, 1962); therefore, the constants in Eq. 13 and 14 are set equal to 23°. A summary of coefficients, their *SE* and P-values are listed in Tables 4 through 6 where all predictors have very small p-values which demonstrate their significance in the models. Removing D_r and p'_o/p_{atm} from Eq. 13 resulted in poor correlations between predicted and measured φ_{cs} values; however, they have small coefficients and SE values where D_r has the smallest SE followed by p'_o/p_{atm} (Table 4). As F increases, particles shape changes close to a sphere and there will be less surface contact between adjacent particles as opposed to platy shape particles (small F value) which is expected to result in smaller φ_{cs} which is obvious from the trend of data in Figure 11a and negative coefficient in Eq. 13. Also, as I_R decreases or as particle R_q increases, one expects more interlocking and an increase in friction between particles which results in a higher φ_{cs} which in manifested in data trend Figure 11b&c. A dense specimen will have more contact between

particles resulting in a higher φ_{cs} when it is compared to a loose specimen (Figure 11e) and positive coefficient for D_r in Eq. 14. These experimental observations show that as particles' morphology deviates from a rounded shape and smooth surface to a more angular and rough one, enhanced interlocking and frictional resistance among contacting particles results in an increase in macroscopic friction and dilatancy angles.

Figure 12 displays models' prediction versus experimental measurements which demonstrate excellent predictions for the measurements that were collected by two independent research groups (Fukushima & Tatsuoka 1984; Lancelot et al. 2006) and this study. ψ model is set to have zero intercept (Eq. 15). To further investigate the relationship between ψ and independent variables in Eq. 15, experimental measurements for very dense sand specimens are plotted in Figure 13 where measurements on glass beads are excluded since they are spherical with smooth surfaces. As D_r increases, ψ increases and as p'_o/p_{atm} increases, ψ decreases which is expected (Figure 13d&e). Figure 13d shows that F-35 sand has the highest ψ followed by #1 dry glass sand, GS#40, Hostun RF, and Toyoura sand. There is a clear trend between I_R and ψ where as I_R increases, ψ increases since particles have more degrees of freedom to rotate when they have rounded corners. Also, as surface texture (R_q) increases, ψ increases, suggesting a higher volume increase as particles interact (sliding and rotation modes) with each order. F has a mixed trend with ψ probably affected by R_q and I_R suggesting a combined effect of R_q, I_R, and F as expressed in Eq. 15.

SUMMARY AND CONCLUSION

Particle morphology plays a significant role in determining the shear strength of granular materials and should be included in predictive models to better predict peak, CS friction angles

and dilatancy angle. In order to identify the effect of particle morphology on the shear strength of granular soils, glass beads and three types of silica sands with different surface characteristics and same gradation were subjected to drained triaxial compression tests at four different confining pressures. Morphologies of the tested particles were characterized by quantifying surface texture index via optical interferometry technique, and roundness, form, and sphericity indices based on 3D high resolution SMT images.

The stress-strain and volume change results of the specimens showed that most specimens exhibited dilative behavior even at relatively high confining pressure (400 kPa) with the rate of dilation is higher as the density increases and as the confining pressure decreases. The impact of particle morphology on shear strength parameters (φ_p, φ_{cs} and ψ) was assessed and simple statistical models were presented to predict ψ, φ_{cs}, and φ_p using particles surface texture (R_q), roundness (I_R), form (F), relative density and normalized mean effective stress as input parameters. As a specimen density decreases and mean stress increases, φ_p, φ_{cs} and ψ decrease. φ_p, φ_{cs} and ψ increase as F and I_R decrease.

Equations 13 through 15 are simple models that can be used to predict friction and dilatancy angles of sand in triaxial experiments using particle morphology, density and initial applied stress. They can be utilized as input for constitutive models to accurately predict the shear strength of granular materials without the need to perform a suite of experiments under different confining pressures and densities.

ACKNOWLEDGMENTS

This material is based on work supported by the National Science Foundation under Grant No. CMMI-1266230. Any opinions, findings, and conclusions or recommendations expressed in

this material are those of the authors and do not necessarily reflect the views of the National Science Foundation. Also, the authors thank Wadi Imseeh for help in statistical analysis.

REFERENCES

Abbireddy, C.O.R., Clayton, C.R.I. (2010). "Varying initial void ratios for DEM simulations." Géotechnique **60**(6), 497–502.

Alsaleh, M. I., Alshibli, K.A., & Voyiadjis, G. Z. (2006). "Influence of Micro-Material Heterogeneity on Strain Localization in Granular Materials." *ASCE: International J. of Geomechanics*, **6**(4), 248-259.

Al-Shibli, K., Macari, E., and Sture, S. (1996). "Digital Imaging Techniques for the Assessment of Homogeneity of Granular Materials." Emerging Technologies in Geotechnical Engineering, Transportation Research Board, Transportation Research Record No. 1526, pp. 121-128, DOI: http://dx.doi.org/10.3141/1526-15

Alshibli, K. A. and Alsaleh, M. (2004) "Characterizing Surface Roughness and Shape of Sands Using Digital Microscopy." *ASCE, Journal of Computing in Civil Engineering*, 18(1), 36-45.

Alshibli, K. A. and Roussel, L. (2006). "Experimental investigation of slip-stick behavior in granular materials." *International Journal for Numerical and Analytical Methods in Geomechanics*, 30(4), 1391-1407, **DOI:** http://dx.doi.org/10.1002/nag.517

Alshibli, K. A., Jarrar, M., Druckrey, A., Al-Raoush, R (2016). "Influence of Particle Morphology on 3D Kinematic Behavior and Strain Localization of Sheared Sand." *ASCE Journal of Geotechnical & Geoenvironmental Engineering,* DOI 10.1061/(ASCE)GT.1943-5606.0001601

Alshibli, K., Druckrey, A. M., Al-Raoush, R., Weiskittel, T., and Lavrik, N. V. (2014). "Quantifying Morphology of Sands using 3D Imaging." *ASCE Journal of Materials in Civil Engineering*, 27(10), 04014275-1 to 04014275-10, DOI: 10.1061/(ASCE)MT.1943-5533.0001246.

ASTM (2016a). Standard test methods for maximum index density and unit weight of soils using a vibratory table, D4253. West Conshohocken, PA: ASTM International.

ASTM (2016b). Standard test methods for minimum index density and unit weight and calculation of relative density, D4254. West Conshohocken, PA: ASTM International.

Batiste, S. N., Alshibli, K. A., Sture, S., and Lankton, M. (2004). "Shear Band Characterization of Triaxial Sand Specimens Using Computed Tomography*" ASTM, Geotechnical Testing Journal*, 27(6), 568-579.

Bolton, M. (1986). "The Strength and Dilatancy of Sands." *Geotechnique*, 36(1), 65-78.

Chakraborty, T. and Salgado, R. (2010). "Dilatancy and shear strength of sand at low confining pressure." *ASCE, J. of Geotechnical and Geoenv. Engineering*, 136(3), 527-532.

Cho, C-C, Dodds, J., and Santamarina, J. C. (2006). "Particle shape effects on packing density, stiffness, and strength: natural and crushed sands" *ASCE, J. of Geotechnical and Geoenv. Engineering,* 132(5), 591-602.

Coulomb, C. A. (1776). "Essai sur une application des règles de maximis & minimis à quelques problèmes de statique, relatifs à l'architecture". De l'Imprimerie Royale.

Duttine, A., Tatsuoka, F., Kongkitkul, W., and Hirakawa, D. (2008). "Viscous behavior of unbound granular materials in direct shear." *Soils and Foundations*, 48(3), 297-318.

Frost, J.D. and Kuo, C.Y. (1996). "Automated Determination of the Distribution of Local Void Ratio from Digital Images." *Geotech. Test. J.*, 19(2), 107-117.

Fukushima, S., and Tatsuoka, F. (1984). "Strength and deformation characteristics of saturated sand at extremely low pressures." *Soils and Foundations,* 24(4), 30-48.

Guo, P. and Su, X. (2007) "Shear Strength, interparticle locking, and dilatancy of granular materials*." Canadian Geotechnical Journal,* 44**,** 579-591.

Hansen, B. (1958). "Line ruptures regarded as narrow rupture zones, basic equations based on kinematic consideration." *Proc. Conf. Earth Pressure Problems,* Brussels, Belgium, 39-51.

Hasan, A. and Alshibli, K. A. (2010). "Discrete Element Simulation of Strength Properties of Johnson Space Center (JSC-1A) Lunar Regolith Simulant." *ASCE, Journal of Aerospace Engineering,* 23(3), 157-165.

Kanatani, K. (1984). "Distribution of Directional Data and Fabric Tensors." *Int. J. Eng. Sci.*, 22(2), 149-164.

Kandasami, R.K., Murthy, T.G. (2015). "Experimental studies on the nfluence of intermediate principal stress and inclination on the mechanical behaviour of angular sands." *Granular Matter*, 17(2), 217–230.

Kandasami, R.K., Murthy, T.G. (2017). "Manifestation of particle morphology on the mechanical behaviour of granular ensembles." *Granular Matter*, 19:21, DOI 10.1007/s10035-017-0703-z

Koener, R. M. (1968). "The Behavior of Cohesionless Materials Formed from Various Materials", Ph.D Dissertation, Duke University, NC.

Konrad, J. M. (1990). "Minimum undrained strength versus steady-state strength of sands." *Journal of Geotechnical Engineering*, 116, 948-963.

Lancelot, L., Shahrour, I, and Al Mahmoud, M. (2006). "Failure and Dilatancy Properties of Sand at Relatively Low Stresses." *ASCE, Journal of Engineering, Mechanics,* 32(12), 1396-1399.

Li, X. S. and Wang, Y. (1998). "Linear Representation of Steady State Line for Sand." *Journal of Geotechnical and Environmental Engineering*, 124(12), 1215-1217.

Lo Presti D., Pedroni S., Crippa V. (1992). "Maximum Dry Density of Cohesionless Soils by Pluviation and by ASTM D 4253-83: A Comparative Study", *ASTM Geotechnical Testing Journal,* 15(2), 180-189.

Manzari, M. T. and Dafalias, Y. F. (1997). "A critical State Two-Surface Plasticity Model for Sands." *Geotechnique*, 47(2), 255-272.

Miura, S. and S. Toki (1982). "A Sample Preparation Method and its Effects on Static and Cyclic Deformation-strength Properties of Sand", *Soils and Foundations, JSSMFE*, 22(1), 61-77.

Powers, M. C. (1982). "Comparison Charts for Estimating Roundness and Sphericity", *AGI Data Sheets*, American Geological Institute.

Oda, M. (1972), "Initial Fabrics and their Relations to Mechanical Properties of Granular Materials", *Soils and Foundations*, 12(1), 18-36.

Rad, N. and M. Tumay (1987). "Factors Affecting Sand Specimen Preparation by Raining", *ASTM Geotechnical Testing Journal,* 10(1), 31-37.

Riemer, M. F., and Seed, R. B. (1997). "Factors Affecting Apparent Position of Steady-State line." *Journal of Geotechnical and Geoenvironmental Engineering*, 123(3), 281-288.

Reynolds, O. (1885). "On the dilatancy of media composed of rigid particles in contact." *Philos. Mag.,* 20(5), 469-485.

Reynolds, O. (1886). "Experiments showing dilatancy, a property of granular material, possibly connected with gravitation. " Proc. Royal Institution of Great Britain, Read February 12, 1886.

Roscoe, K. (1970). "The Influence of Strains in Soil Mechanics." *Geotechnique*, 20(2), 129-170.

Rowe, P. W. (1962). "The Stress-Dilatancy Relation for Static Equilibrium of an Assembly of Particles in Contact." *Proceedings of the Royal Society,* A269, 500-527.

Shipton, B., and Coop, M. R. (2014). "Transitional behaviour in sands with plastic and non-plastic fines." *Soils and Foundations, 55(1): 1-16,* http://doi.org/10.1016/j.sandf.2014.12.001

Sukumaran, B., and Ashmawy, A. K. (2001). "Quantitative characterisation of the geometry of discret particles." Géotechnique, 619-627.

Tatsuoka, F. (1987). Discussion: The Strength and Dilatancy of Sands." *Geotechnique*, 37(2), 219-226.

Vardoulakis, I. and Graf, B. (1985). "Calibration of Constitutive Models for Granular Materials Using Data from Biaxial Experiments." *Geotechnique*, 35(3), 299-317.

Vermeer, P. (1978). "A Double Hardening Model for Sand." *Geotechnique*, 28(4), 413-433.

Vermeer, P.A., and de Borst, R. (1984). "Non-associated Plasticity for Soils, Concrete and Rock", Heron, 29 (3), 3-64.

Wadell, H. (1932). “Volume Shape and Roundness of Rock Particles.” *Journal of geology*, 40, 443-488.

Wood, D. M. (1990). *Soil behaviour and critical state soil mechanics*. Press Syndicate of the University of Cambridge the Pitt Building, New York, NY 10011, USA.

Zavala, J. M. R. (2012). “Particle Shape Quantities and Influence on Geotechnical Properties - A Review.” Ph.D. , Luleå University of Technology Luleå , Sweeden.

Table 1. Source and properties of sands used in this study

Material	G_s	d_{50} (mm)	ASTM D4253 e_{min}	ASTM D4254 e_{max}	Al-Shibli et al. (1996) e_{min_A}	Source	Supplier	Grain Size
F-35 Ottawa Sand	2.650	0.36	0.570	0.763	0.490	Ottawa, IL, USA	US Silica Company	Size portion between US sieves #40 (0.42 mm) and #50 (0.297 mm)
#1 Dry Glass Sand	2.650	0.36	0.715	0.947	0.626	Berkeley Springs, WV, USA		
GS#40 Columbia Grout Sand	2.650	0.36	0.693	0.946	0.643	Columbia, SC, USA		
Glass beads	2.550	0.36	0.686	0.800	0.565	Soda lime glass	Jaygo inc.	
Hostun RF Sand	2.658[+]	0.34	0.592[+]	0.978[+]	NA	France	Prof. Viggiani	Figure 2
Toyoura Sand	2.648[++]	0.22	0.606[+] [+]	0.977[++]	NA	Japan	Prof. Tatsuoka	Figure 2

[+] Duttine et al. (2008)
[++] Fukushima & Tatsuoka (1984)

Table 2. Mean values of morphology indices and their standard deviations (SD).

Material	N[+]	I_{sph}		I_R		R_q (μm)		Form (F)
		Mean	SD	Mean	SD	Mean	SD	Mean
F-35 Ottawa Sand	712	1.872	0.732	0.959	0.083	2.084	1.693	0.614
#1 Dry Glass Sand	1063	1.704	0.859	0.937	0.106	1.990	1.135	0.589
GS#40 Columbia Grout Sand	1069	1.674	0.799	0.924	0.099	1.923	1.986	0.597
Glass beads	1240	1.096	0.433	0.965	0.043	0.381	0.947	0.930
Hostun RF Sand	888	1.833	0.971	0.904	0.136	1.972	1.001	0.558
Toyoura Sand	760	1.665	0.579	0.906	0.097	1.847	0.932	0.578

[+] number of particles used to calculate I_{sph}, I_R, $and\ F$

Table 3.Summary of the measured friction and dilatancy angles for the experiments.

Material	State	σ_3 (kPa)	$\gamma_d{}^+$ (g/cm^3)	e	D_r (%)	φ_p (deg.)	ϕ_{cs} (deg.)	ψ (deg.)	% fracured Sand
Glass Beads	Loose	15	1.48	0.788	5.1	NA	27.9	3.9	
		50	1.48	0.795	2.1	NA	26.7	1.2	
		100	1.48	0.792	3.4	NA	26.0	2.0	
		400	1.49	0.780	8.5	NA	24.7	2.1	2.9
	Medium dense	15	1.55	0.707	39.6	31.8	28.5	10.8	
		50	1.55	0.706	40.0	30.8	28.2	11.2	
		100	1.54	0.721	33.6	29.7	26.9	9.7	
		400	1.56	0.701	42.1	29.9	26.3	8.9	2.2
	Very dense	15	1.63	0.624	74.9	38.7	31.3	20.9	
		50	1.63	0.622	75.7	37.3	29.8	20.2	
		100	1.64	0.612	80.0	37.2	29.6	20.2	
		400	1.63	0.621	76.2	34.4	28.9	17.8	3.7
F-35 Ottawa sand	Loose	15	1.53	0.735	10.3	NA	33.9	2.5	
		50	1.53	0.731	11.7	NA	32.1	2.4	
		100	1.54	0.726	13.6	NA	31.9	2.4	
		400	1.52	0.738	9.2	NA	30.8	2.3	0.29
	Medium dense	15	1.64	0.617	53.5	39.7	35.7	10.0	
		50	1.64	0.612	55.3	37.2	33.9	10.4	
		100	1.64	0.611	55.7	37.0	33.0	10.6	
		400	1.64	0.615	54.2	35.9	31.7	10.0	0.24
	Very dense	15	1.78	0.491	99.6	46.8	39.4	21.7	
		50	1.77	0.496	97.8	44.6	37.2	20.6	
		100	1.77	0.498	97.1	43.7	35.3	20.0	
		400	1.78	0.491	99.6	41.9	33.1	19.3	0.34
GS#40 Columbia Grout Sand	Loose	15	1.38	0.921	8.3	NA	36.4	2.4	
		50	1.38	0.916	9.9	NA	33.8	2.8	
		100	1.37	0.933	4.3	NA	33.1	1.9	
		400	1.38	0.915	10.2	NA	32.2	1.3	7.4
	Medium dense	15	1.50	0.764	60.1	40.7	37.7	11.7	
		50	1.50	0.762	60.7	38.5	35.0	11.0	
		100	1.51	0.758	62.0	37.9	34.3	11.0	
		400	1.50	0.762	60.7	36.6	33.7	9.1	7.6
	Very dense	15	1.62	0.638	101.7	45.9	41.1	20.4	
		50	1.61	0.648	98.3	44.3	37.3	19.6	
		100	1.62	0.635	102.6	43.2	35.9	18.7	
		400	1.62	0.634	103.0	41.8	35.2	17.2	7.3

Table 3 (continue)

Material	State	σ_3 (kPa)	$\gamma_d{}^+$ (g/cm^3)	e	D_r (%)	φ_p (deg.)	ϕ_{cs} (deg.)	ψ (deg.)	% fracured Sand
#1 Dry Glass	Loose	15	1.37	0.935	3.7	NA	35.4	2.4	
		50	1.38	0.916	9.7	NA	33.2	1.9	
		100	1.37	0.935	3.7	NA	32.9	1.6	
		400	1.38	0.925	6.9	NA	32.0	1.4	12.3
	Medium dense	15	1.49	0.777	53.0	39.2	37.0	10.3	
		50	1.48	0.786	50.2	37.6	34.3	9.6	
		100	1.49	0.774	53.9	37.8	33.6	10.3	
		400	1.49	0.775	53.6	36.4	33.2	8.5	11.4
	Very dense	15	1.62	0.635	97.2	47.6	40.6	21.1	
		50	1.62	0.639	96.0	44.5	37.4	19.7	
		100	1.61	0.645	94.1	43.8	36.5	19.1	
		400	1.62	0.631	98.4	42.4	35.4	17.7	12.2
Hostun RF Sand[+]	Loose	20	1.40	0.901	11.5	NA	39.8	1.7	Not reported
		50	1.41	0.884	16.1	NA	37.7	1.9	
		100	1.41	0.880	17.1	NA	35.8	1.3	
	Very dense	20	1.65	0.610	90.4	49.8	41.3	23.3	Not reported
		50	1.65	0.614	89.4	46.5	39.6	17.6	
		100	1.65	0.614	89.4	45.1	38.7	17.2	
Toyoura Sand[++]	Loose	21	1.45	0.827	40.3	NA	37.9	5.2	Not reported
		50	1.45	0.831	39.2	NA	36.3	5.2	
		99	1.45	0.829	39.8	NA	35.6	3.9	
		197	1.45	0.829	39.8	NA	35.1	3.5	
	Very Dense	21	1.60	0.658	85.8	43.9	37.9	13.5	Not reported
		50	1.60	0.658	85.8	43.0	36.3	15.0	
		99	1.58	0.671	82.3	42.2	39.5	11.5	
		197	1.58	0.677	80.6	40.5	38.5	13.3	

[+]Lancelot et al. (2006)

[++] Fukushima & Tatsuoka (1984)

Table 4. Results of multivariable statistical model for critical state friction angle φ_{cs}

Predictor	Coefficient (β)	SE	P value
F	-134.06	22.70	2.05×10^{-7}
I_R	142.04	23.56	1.29×10^{-7}
R_q	-21.02	4.31	9.01×10^{-6}
p_o'/p_{atm}	-0.861	0.136	4.41×10^{-8}
D_r	0.043	0.005	1.69×10^{-10}
Statistical Constant	23	NA	NA

Table 5. Results of multivariable statistical model for peak friction angle φ_p

Predictor	Coefficient (β)	SE	P value
F	-62.90	25.90	0.0209
I_R	67.00	26.96	0.0180
R_q	-9.021	4.889	0.0738
p_o'/p_{atm}	-0.932	0.148	3.63×10^{-7}
D_r	0.160	0.011	1.94×10^{-16}
Statistical Constant	23	NA	NA

Table 6. Results of multivariable statistical model for dilatancy angle ψ

Predictor	Coefficient (β)	SE	P value
F	77.72	27.00	0.0056
I_R	-76.35	28.02	0.0085
R_q	12.77	5.13	0.0157
p_o'/p_{atm}	-0.486	0.162	0.0041
D_r	0.196	0.0075	1.11×10^{-36}
Statistical Constant	0	NA	NA

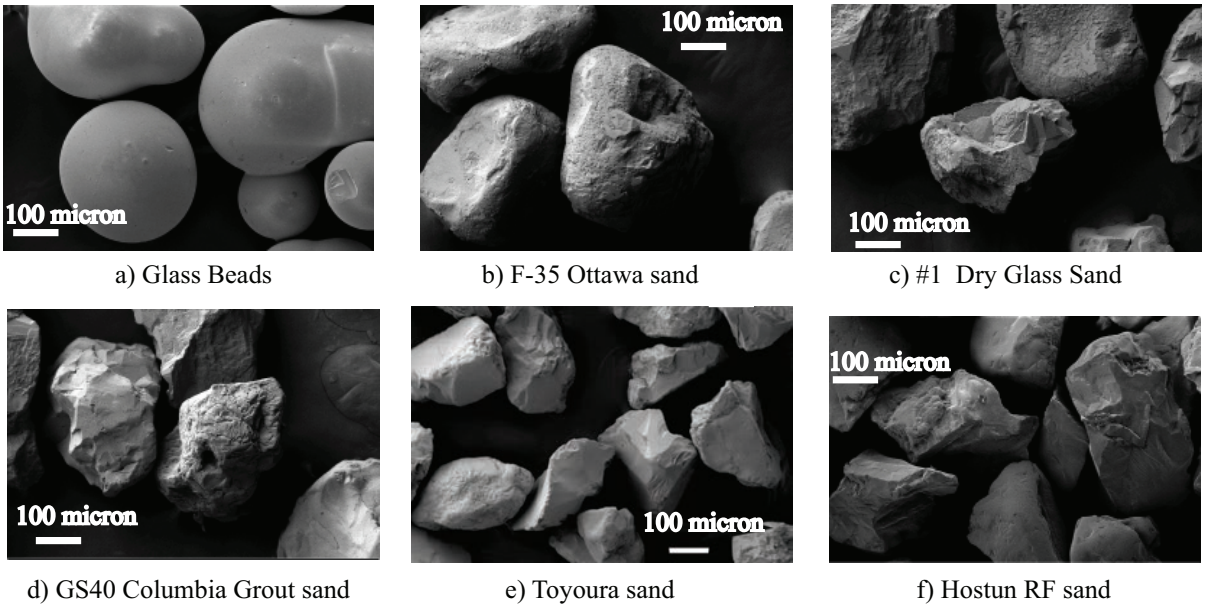

a) Glass Beads b) F-35 Ottawa sand c) #1 Dry Glass Sand

d) GS40 Columbia Grout sand e) Toyoura sand f) Hostun RF sand

Figure 1. SEM images of glass beads and sand

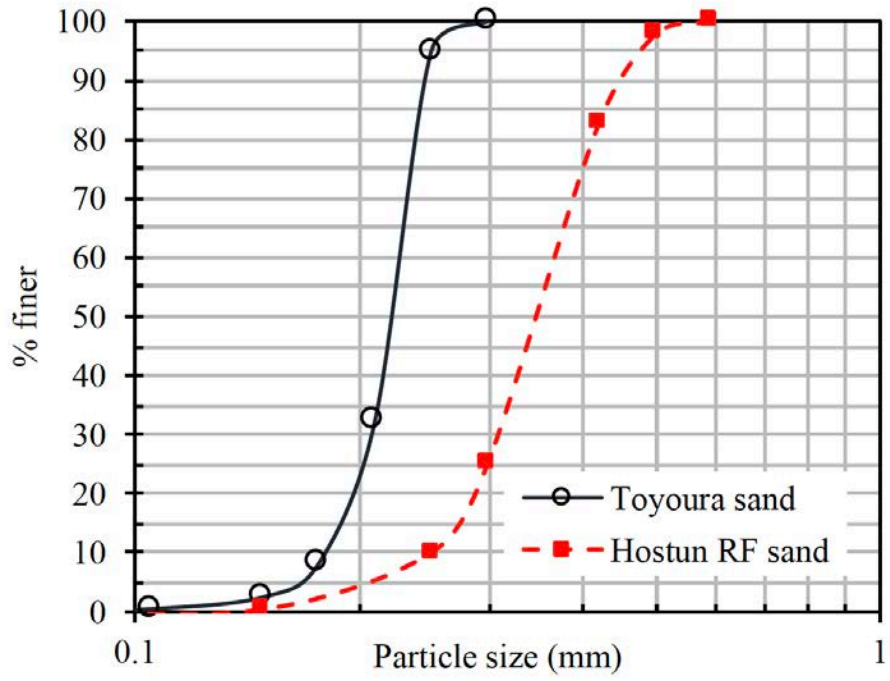

Figure 2. Grain size distribution curves for Hostun RF and Toyoura sands

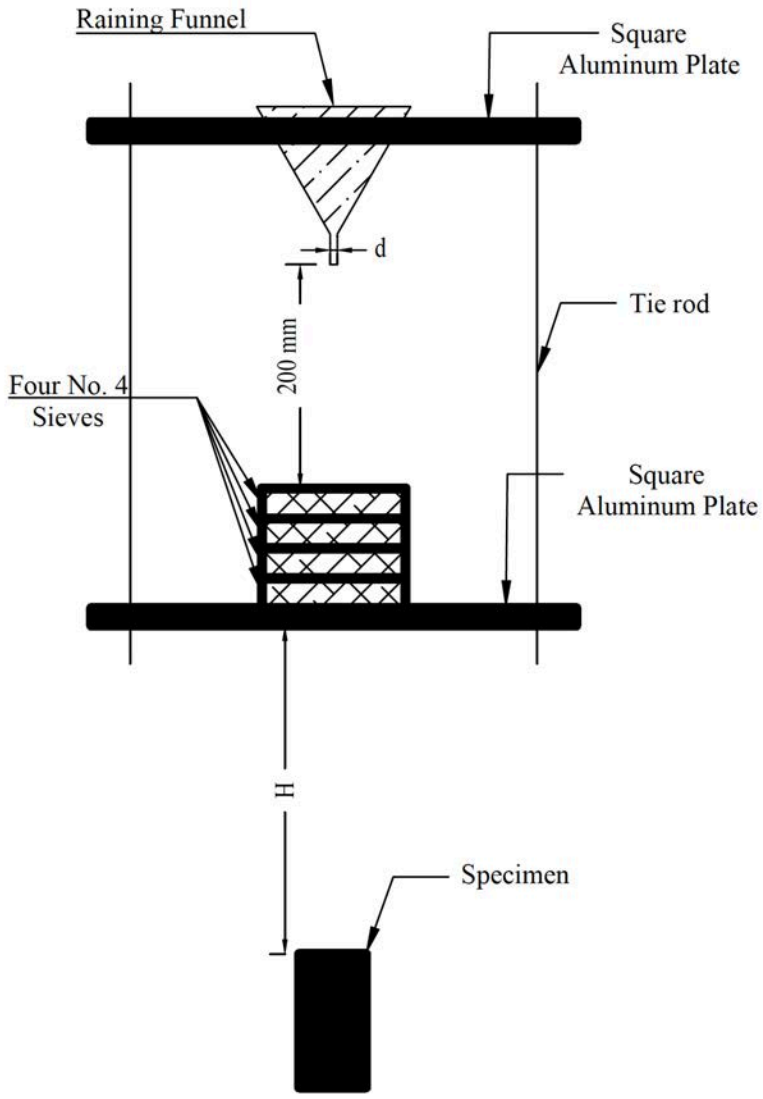

Figure 3. Schematic of air pluviation apparatus

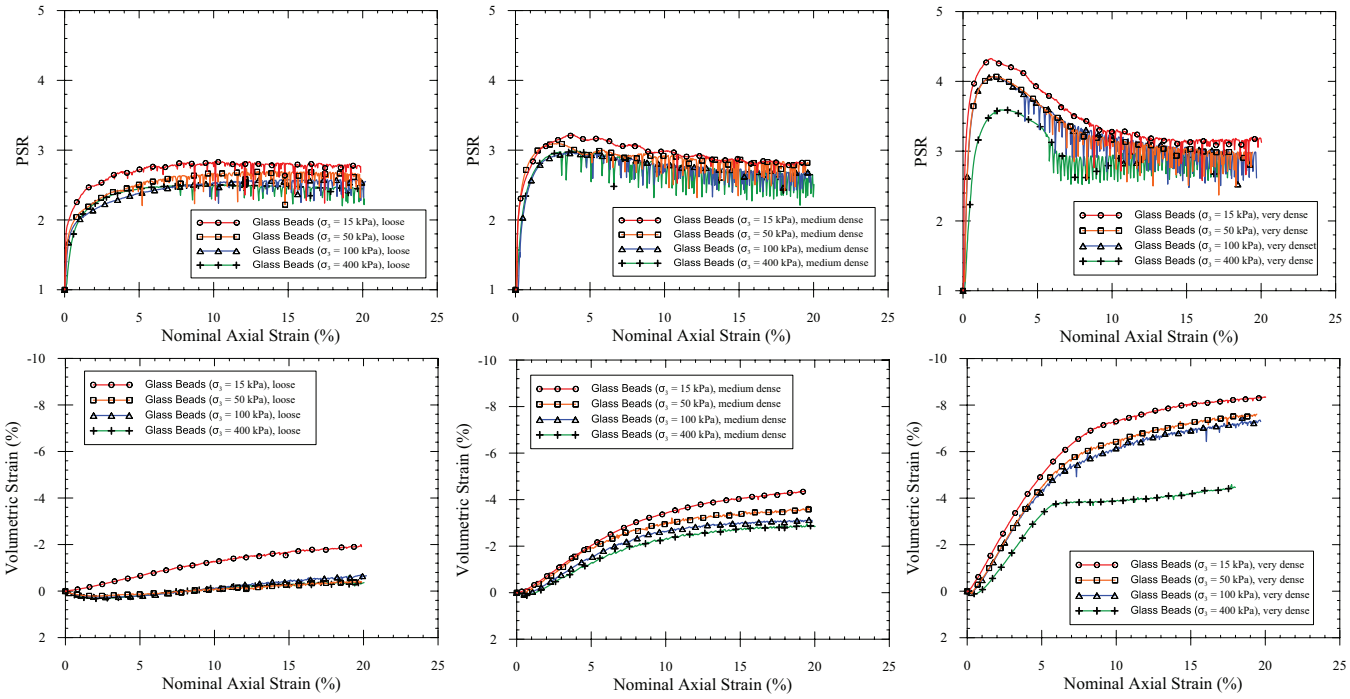

(a) Loose specimens (b) Medium dense specimens (c) Very dense specimens

Figure 4. Principal Stress Ratio versus Axial Strain and Volumetric Strain versus Axial Strain Responses for glass beads

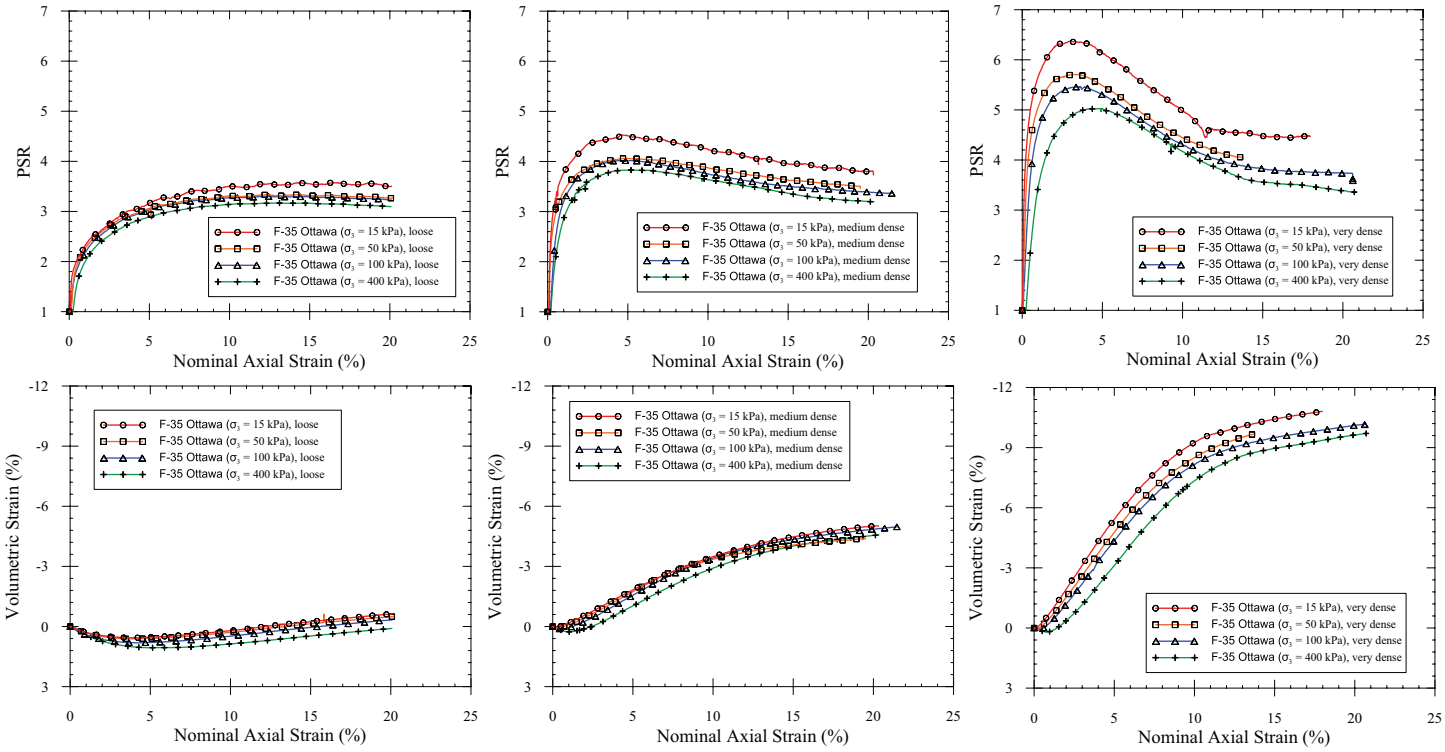

(a) Loose specimens (b) Medium dense specimens (c) Very dense specimens

Figure 5. Principal Stress Ratio versus Axial Strain and Volumetric Strain versus Axial Strain Responses for F-35 Ottawa sand

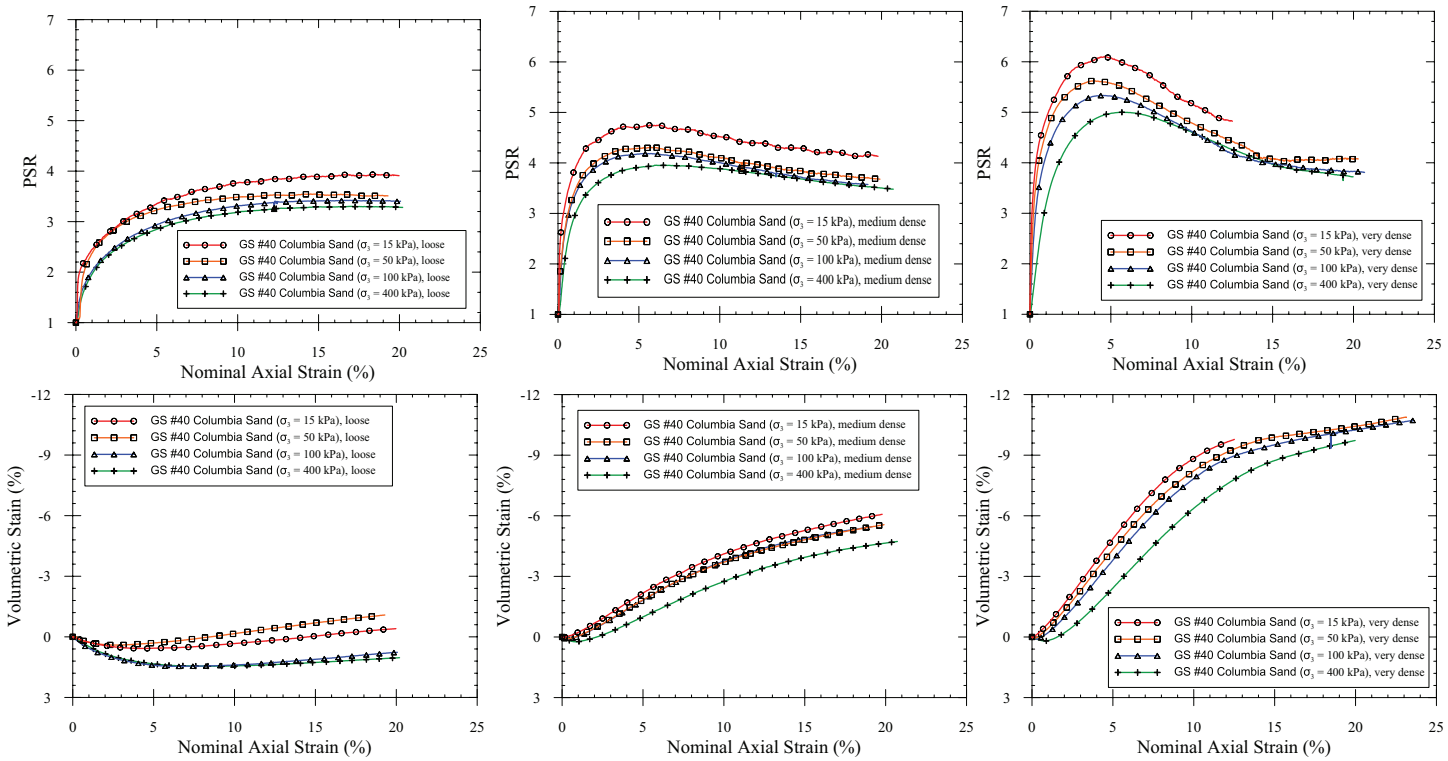

(a) Loose specimens (b) Medium dense specimens (c) Very dense specimens

Figure 6. Principal Stress Ratio versus Axial Strain and Volumetric Strain versus Axial Strain Responses for GS#40 Columbia Grout Sand

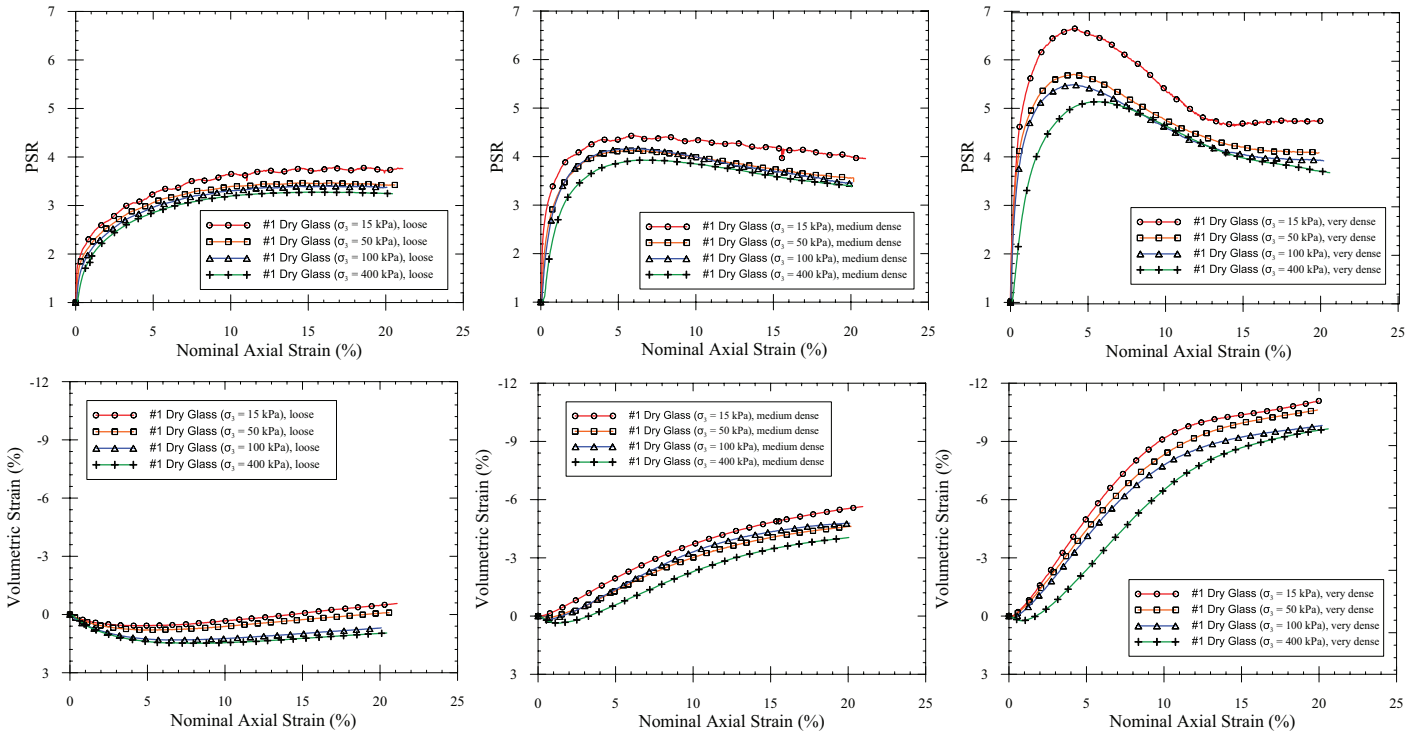

(a) Loose specimens (b) Medium dense specimens (c) Very dense specimens

Figure 7. Principal Stress Ratio versus Axial Strain and Volumetric Strain versus Axial Strain Responses for #1 Dry Glass Sand

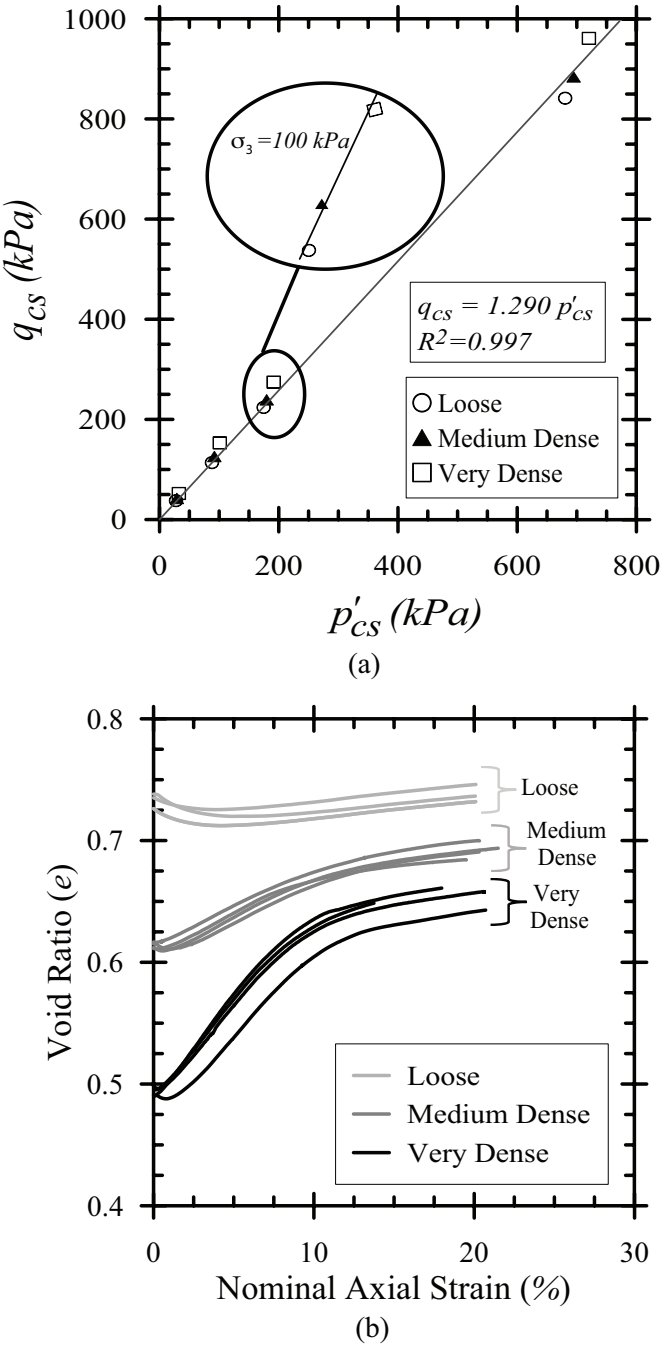

Figure 8. (a) Relationship between mean effective stress and deviator stress at the CS for F35 sand; (b) variation of void ratio with nominal axial strain for F35 sand

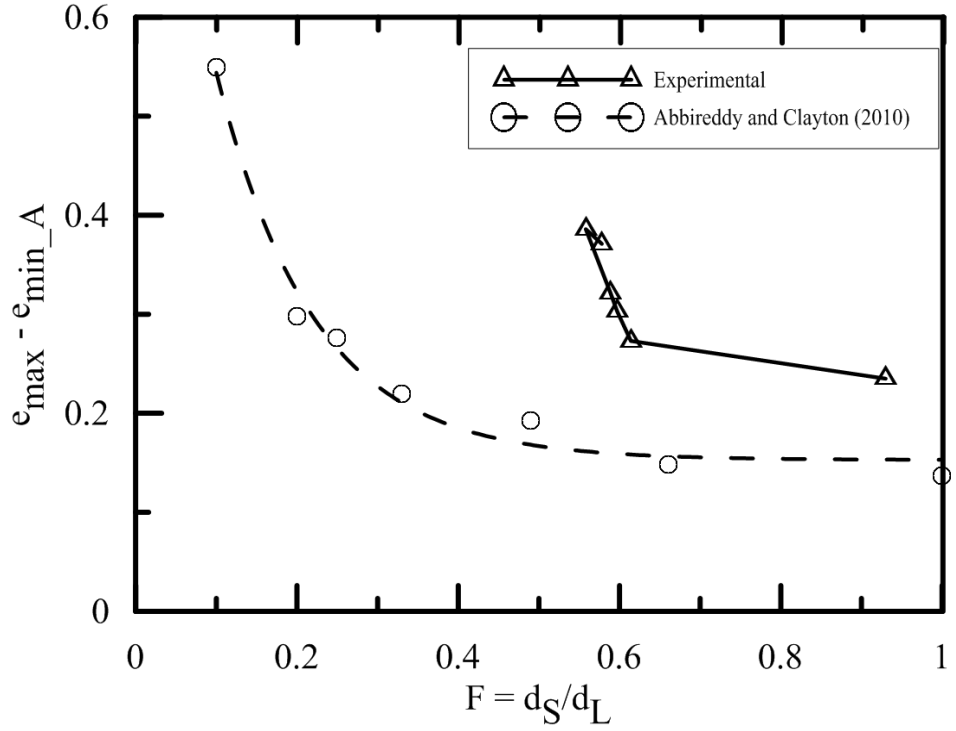

Figure 9. Variation of void ratios with respect to particle form.

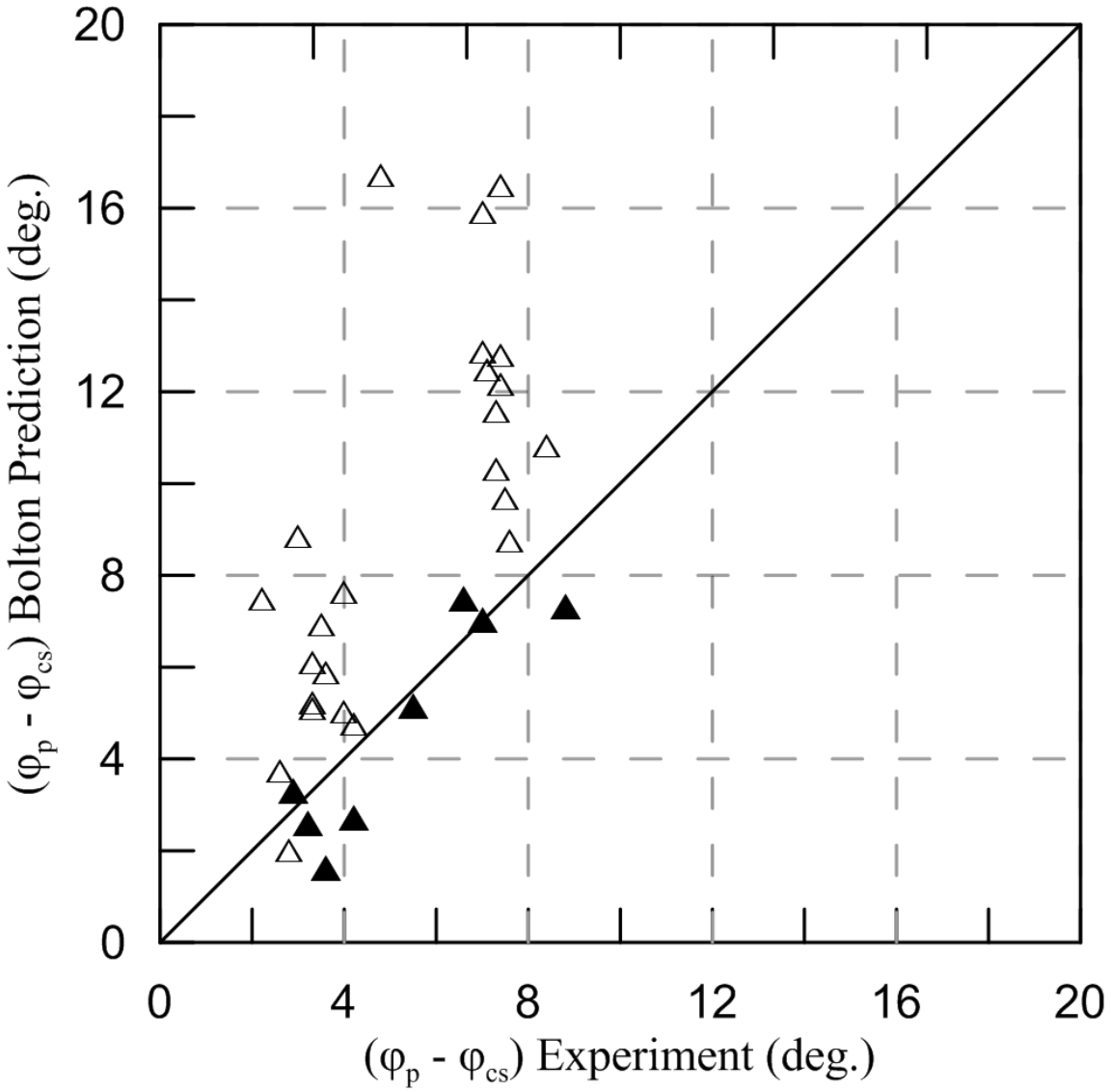

Figure 10. Bolton (1986) prediction versus experimental measurements of $\varphi_p - \varphi_{cs}$ (filled triangles represent conducted at 400 kPa confining pressure)

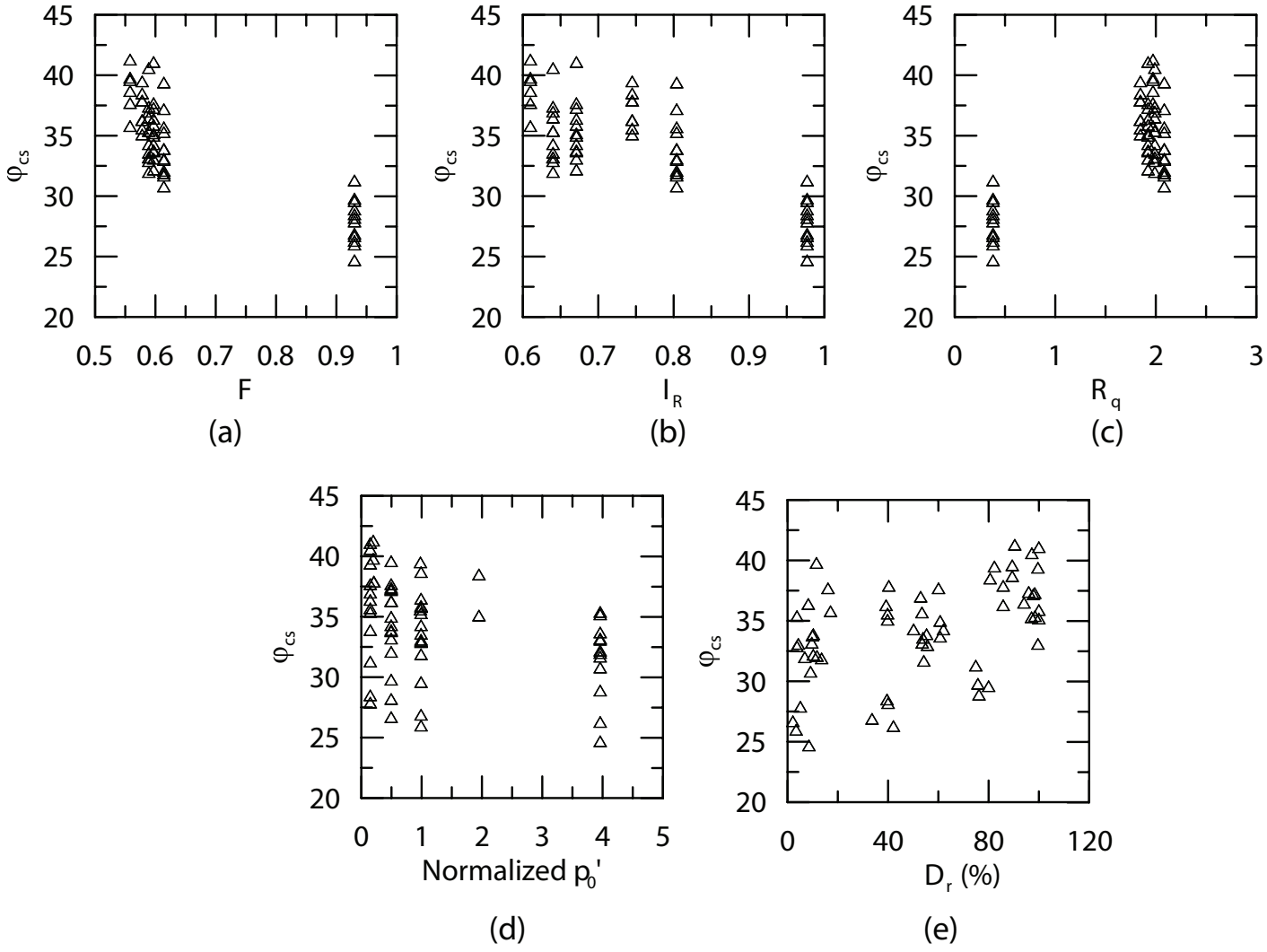

Figure 11. Statistical assessment for the influence of (a) Form (F); (b) roundness (I_R); (c) surface texture (R_q); (d) normalized mean effective stress (p_o'/p_{atm}); and (e) specimen relative density (D_r) on critical state friction angle (φ_{cs}).

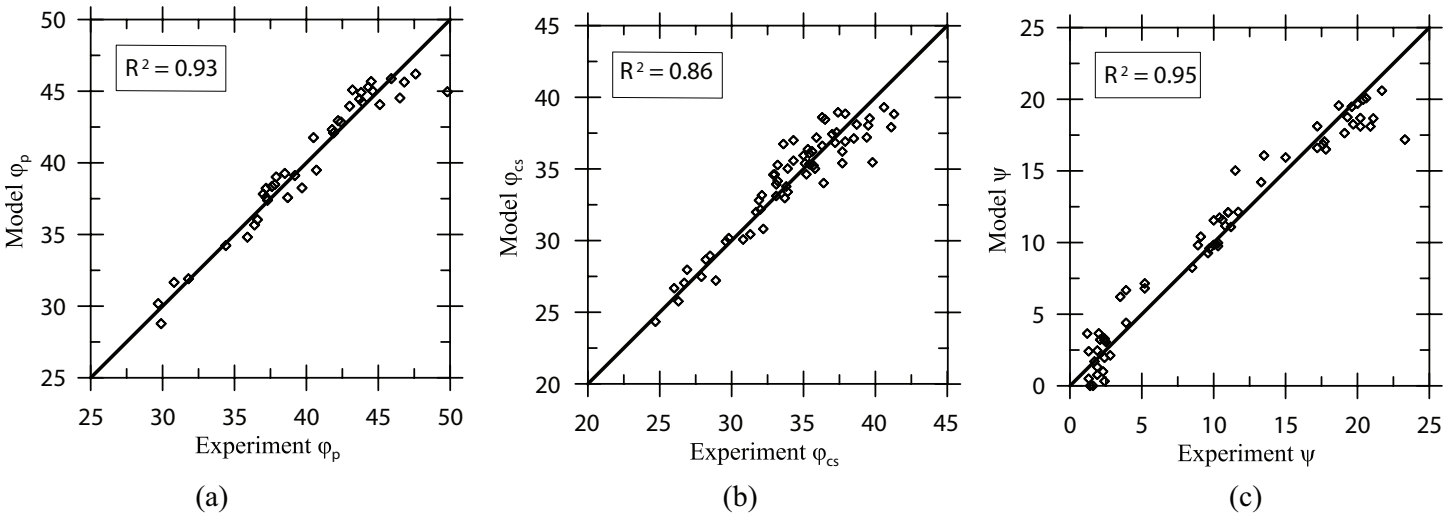

Figure 12. Experiments versus models' predictions for (a) peak state friction angle (φ_p); (b) critical state friction angle (φ_{cs}); and (c) dilatancy angle ψ

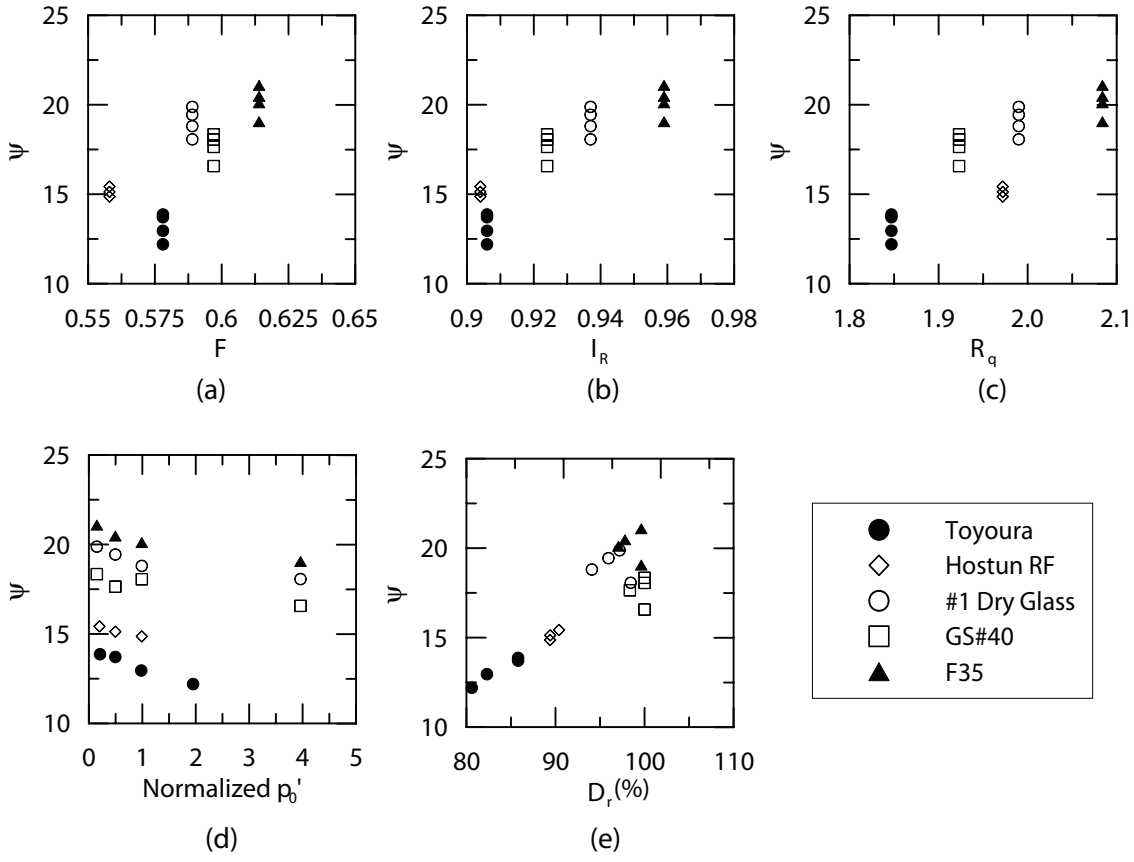

Figure 13. Statistical assessment for the influence of (a) Form (F); (b) roundness (I_R); (c) surface texture (R_q); (d) normalized mean effective stress (p'_o/p_{atm}); and (e) specimen relative density (D_r) on dilatancy angle (ψ) for very dense specimens excluding glass beads.